Multicritical behavior of the Ising metamagnet in both external longitudinal and transverse fields

Guozhu Wei,[1,2,*] Jing Liu,[1] Hailing Miao,[1] and An Du[1]
[1]*College of Sciences, Northeastern University, Shenyang 110004, China*
[2]*International Center for Material Physics, Academia Sinica, Shenyang 110015, China*
(Received 26 April 2007; published 1 August 2007)

A two-sublattice Ising metamagnet in both external longitudinal and transverse fields is studied within the mean-field approach based on Bogoliubov's inequality for the Gibbs free energy. At finite temperatures, by changing values of the parameters of the model many different types of phase diagrams in the longitudinal field-temperature plane and in the transverse field-temperature plane are determined. The results show that the tricritical point can occur and decomposes into a critical end point and a double critical end point in a certain small region of the external longitudinal and transverse fields. The temperature of the tricritical point monotonically increases with decreasing the transverse magnetic field Ω and increasing the longitudinal magnetic field h. A line of fourth-order critical points is also determined.

DOI: 10.1103/PhysRevB.76.054402 PACS number(s): 75.30.Kz, 75.10.Jm, 75.30.Gw

I. INTRODUCTION

An ideal metamagnet is made up of identical plane layers of spins, with ferromagnetic couplings between the spins in each layer but antiferromagnetic couplings between adjacent layers. In a zero external field, a metamagnet behaves as an Ising-like antiferromagnet. $FeCl_2$ and $FeBr_2$ are well-known metamagnets of Ising type. The phase diagram of metamagnetic systems in the external longitudinal field versus temperature plane has been studied both theoretically[1–10] and experimentally.[11–14] Theoretically, in mean-field theory, the Ising metamagnet is known to display two kinds of phase diagrams in the (T,H) plane,[1] depending on the ratio $R=Z_1J_1/Z_2J_2$. The Z_1 and $Z_2(J_1,J_2)$ are the numbers of nearest neighbors (exchange coupling) in the plane and in adjacent planes, respectively. In both cases, the transition between the antiferromagnetic and paramagnetic phases is of first order at low temperature and large longitudinal fields, while it is second order at higher temperature. When $R<-3/5$, the two types of transitions are connected by a tricritical point. When $R>-3/5$, the tricritical point decomposes into a critical end point and a double critical end point. Kincaid and Cohen predicted that new types of critical behavior may be observed in $FeBr_2$ and other similar systems from a study of a simple mean-field model for metamagnets.[15] Selke and Pleimling[5,6] studied anomalies of the magnetization and the specific heat by using the mean-field theory and the Monte Carlo simulations for the cases $s=1/2$ and $s=1$, respectively. In particular, the dependence of the anomaly behavior on competing intralayer interactions, the spin value, and the Ising-like anisotropy are investigated. Wang and Rauchwarger[16] and Wang and Kimel[17] showed that a fourth-order critical point along with other critical points of lower order prevails in the $s=1$ antiferromagnetic Blume-Capel model in the mean-field approximation and by using Monte Carlo simulations for the simple cubic lattice. The observation of the fourth-order criticality is also discussed. They proposed to observe the fourth-order critical point in a transverse field.

Recently, Žukovič and Bobak and Žukovič and Idogaki studied the phase diagrams and tricritical behavior of a diluted Ising metamagnet in an external longitudinal field by the use of an effective-field theory with correlation[8] and Monte Carlo simulation,[9] respectively, and examined the behavior of the tricritical point as a function of dilution and ratio of interplane-intraplane interactions. Moreira *et al.*[10] studied compressible metamagnetic Ising model within the mean-field Curie-Weiss approach and found that three different possibilities arise for the behavior of the tricritical point under pressure. Žukovič and Idogaki[18] studied multicritical properties of an $s=1/2$ Ising metamagnet in an external field by using Monte Carlo simulations and observed only tricritical behavior with no signs of the decomposition. Galam *et al.*[19] studied the phase diagram of an Ising metamagnet in the presence of a uniform and a random field. Using the mean-field theory, they showed that the qualitative features of the phase diagrams are significantly dependent on the distribution of the random fields.

Experimentally, in the temperature range between the critical end point and the double critical end point, Petracic *et al.*[20] observed a sharp peak in magnetization measurements under a field inclined by 33° with the c axis (perpendicular to the plane) of the crystal $FeBr_2$. They concluded that the peak was affected by the ordering of the planar spin components. It is obvious that the field can be decomposed into the longitudinal (perpendicular to the plane) and transverse (parallel to the plane) fields.

On the other hand, the critical and magnetic properties of the spin-1/2 transverse Ising model and the mixed two-sublattice Ising model in the external transverse field have also been studied by using the mean-field approximation[21,22] and the effective-field theory.[23,24] Recently, Ovchinnikov *et al.*[25] studied the antiferromagnetic Ising chain in a mixed transverse and longitudinal magnetic field by using the classical approach and the density-matrix renormalization-group method and given the ground-state phase diagram in (h_x,h_y) plane. These investigations show that the transition temperature falls to zero at a certain transverse field. However, up to now few people, as far as we know, have studied Ising meta-

magnet in both external longitudinal and transverse fields. In this work, we extend the mean-field theory to Ising metamagnet in both external longitudinal and transverse fields. The purpose is to investigate the phase diagrams of Ising metamagnet in both external longitudinal and transverse fields. Specifically, the effect of the external transverse field on the tricritical behavior of the Ising metamagnet is studied.

The paper is organized as follows. In Sec. II, a precise definition of the model is given, and relevant expressions in the mean-field approximation are derived. In Sec. III, the numerical results and discussions are given. The conclusions are given in Sec. IV.

II. MODEL AND METHODS

We consider a two-sublattice Ising metamagnet in both longitudinal and transverse magnetic fields. The Hamiltonian of the system is given by

$$H = -J_1\left(\sum_{\langle i,j\rangle} s_i^z s_j^z + \sum_{\langle k,l\rangle} s_k^z s_l^z\right) - J_2 \sum_{\langle i,k\rangle} s_i^z s_k^z - H_z\left(\sum_i s_i^z + \sum_k s_k^z\right) - H_x\left(\sum_i s_i^x + \sum_k s_k^x\right), \tag{1}$$

where s_i^μ ($\mu = x, z$) denotes the μ component of a spin variable, $s_i^z = \pm 1$. In the system, odd planes and even planes constitute sublattice A and sublattice B, respectively. $\langle i,j\rangle$ (belong to sublattice A) and $\langle k,l\rangle$ (belong to sublattice A) denote the nearest neighbor pairs in the plane and $\langle i,k\rangle$ denote the nearest neighbor pairs in adjacent planes (between sublattices A and B). H_z and H_x denote the longitudinal (perpendicular to the plane) and the transverse (parallel to the plane) magnetic field. In the calculation, we assume $J_1 > 0$ and $J_2 < 0$ so that each of the planes is ferromagnetic, but antiferromagnetic coupled to adjacent planes.

According to the procedure outlined in Ref. 19 for a two-sublattice Ising metamagnet in uniform and random fields, we can obtain the conditions determining the transition temperature and the tricritical point of the system. First, we derive the mean-field equations from Bogoliubov's variational principle for Gibbs free energy,[26]

$$G(H) \leqslant \Phi = G_0(H_0) + \langle H - H_0\rangle_0, \tag{2}$$

where $G(H)$ is the true free energy of the system described by the Hamiltonian (1), $G_0(H_0)$ is the free energy of a trial Hamiltonian H_0 which depends on variational parameters, and $\langle H - H_0\rangle_0$ denotes a thermal average over the ensemble defined by H_0.

Choosing the noninteracting trial Hamiltonian

$$H_0 = -(\gamma_A + H_z)\sum_{i\in A} s_i^z - H_x \sum_{i\in A} s_i^x - (\gamma_B + H_z)\sum_{k\in B} s_k^z - H_x \sum_{k\in B} s_k^x, \tag{3}$$

where γ_A and γ_B are the two variational parameters. By using the rotation transformation,[27] we obtain

$$G(H) \leqslant \Phi = -\frac{N}{2\beta}\{\ln[2\cosh(\beta\sqrt{(\gamma_A + H_z)^2 + H_x^2})] + \ln[2\cosh(\beta\sqrt{(\gamma_B + H_z)^2 + H_x^2})]\} + \frac{N}{2}\left[\left(\gamma_A - \frac{1}{2}Z_1 J_1 m_A - \frac{1}{2}Z_2 J_2 m_B\right)m_A + \left(\gamma_B - \frac{1}{2}Z_1 J_1 m_B - \frac{1}{2}Z_2 J_2 m_A\right)m_B\right], \tag{4}$$

where $\beta = 1/k_B T$ and N is the total number of sites of the system. The longitudinal and transverse sublattice magnetizations m_A, m_B and m_A^x, m_B^x per spin are defined by

$$m_A \equiv \langle s_i^z\rangle_0 = \frac{\gamma_A + H_z}{\sqrt{(\gamma_A + H_z)^2 + H_x^2}} \tanh(\beta\sqrt{(\gamma_A + H_z)^2 + H_x^2}), \tag{5}$$

$$m_B \equiv \langle s_k^z\rangle_0 = \frac{\gamma_B + H_z}{\sqrt{(\gamma_B + H_z)^2 + H_x^2}} \tanh(\beta\sqrt{(\gamma_B + H_z)^2 + H_x^2}), \tag{6}$$

$$m_A^x \equiv \langle s_i^x\rangle_0 = \frac{H_x}{\sqrt{(\gamma_A + H_z)^2 + H_x^2}} \tanh(\beta\sqrt{(\gamma_A + H_z)^2 + H_x^2}), \tag{7}$$

$$m_B^x \equiv \langle s_k^x\rangle_0 = \frac{H_x}{\sqrt{(\gamma_B + H_z)^2 + H_x^2}} \tanh(\beta\sqrt{(\gamma_B + H_z)^2 + H_x^2}). \tag{8}$$

Now, by minimizing the right-hand side of inequality (4) with respect to γ_A and γ_B, we determine the variational parameters in the form

$$\gamma_A = Z_1 J_1 m_A + Z_2 J_2 m_B, \tag{9}$$

$$\gamma_B = Z_1 J_1 m_B + Z_2 J_2 m_A, \tag{10}$$

where Z_1 and Z_2 are the coordination numbers of nearest neighbors in the plane and in adjacent planes, respectively.

In order to determine analytically some features of the phase diagram, we introduce longitudinal total magnetization, staggered magnetization, as done in Ref. 19, and transverse total magnetization,

$$M_t = \frac{1}{2}(m_A + m_B), \tag{11}$$

$$M_s = \frac{1}{2}(m_A - m_B), \tag{12}$$

$$M_x = \frac{1}{2}(m_A^x + m_B^x), \tag{13}$$

and the reduced quantities

$$t = \frac{1}{\beta(Z_1J_1 - Z_2J_2)}, \quad h = \frac{H_z}{Z_1J_1 - Z_2J_2}, \quad \Omega = \frac{H_x}{Z_1J_1 - Z_2J_2}, \tag{14a}$$

$$\alpha = \frac{Z_1J_1 + Z_2J_2}{Z_1J_1 - Z_2J_2} = \frac{R+1}{R-1}, \tag{14b}$$

where $R = Z_1J_1/Z_2J_2$.

Inserting Eqs. (9) and (10) into the right-hand side of Eqs. (4)–(8) and using Eqs. (11)–(14), we arrive at the mean-field equations

$$M_t = \frac{1}{2}\left[\frac{h + \alpha M_t + M_s}{\sqrt{(h + \alpha M_t + M_s)^2 + \Omega^2}} \tanh \frac{\sqrt{(h + \alpha M_t + M_s)^2 + \Omega^2}}{t} + \frac{h + \alpha M_t - M_s}{\sqrt{(h + \alpha M_t - M_s)^2 + \Omega^2}} \tanh \frac{\sqrt{(h + \alpha M_t - M_s)^2 + \Omega^2}}{t}\right], \tag{15}$$

$$M_s = \frac{1}{2}\left[\frac{h + \alpha M_t + M_s}{\sqrt{(h + \alpha M_t + M_s)^2 + \Omega^2}} \tanh \frac{\sqrt{(h + \alpha M_t + M_s)^2 + \Omega^2}}{t} - \frac{h + \alpha M_t - M_s}{\sqrt{(h + \alpha M_t - M_s)^2 + \Omega^2}} \tanh \frac{\sqrt{(h + \alpha M_t - M_s)^2 + \Omega^2}}{t}\right], \tag{16}$$

$$M_x = \frac{1}{2}\left[\frac{\Omega}{\sqrt{(h + \alpha M_t + M_s)^2 + \Omega^2}} \tanh \frac{\sqrt{(h + \alpha M_t + M_s)^2 + \Omega^2}}{t} + \frac{\Omega}{\sqrt{(h + \alpha M_t - M_s)^2 + \Omega^2}} \tanh \frac{\sqrt{(h + \alpha M_t - M_s)^2 + \Omega^2}}{t}\right]. \tag{17}$$

Then, the mean-field free energy per spin is identified with the lower limit of inequality (4) and may be written as

$$f = \frac{\Phi}{N(Z_1J_1 - Z_2J_2)} = -\frac{t}{2}\left\{\ln\left[2\cosh\frac{\sqrt{(h + \alpha M_t + M_s)^2 + \Omega^2}}{t}\right] + \ln\left[2\cosh\frac{\sqrt{(h + \alpha M_t - M_s)^2 + \Omega^2}}{t}\right]\right\} + \frac{\alpha}{2}M_t^2 + \frac{1}{2}M_s^2. \tag{18}$$

It can get analytic solution for second-order transition point and tricritical point. The order parameter, which is used to describe the transition of Ising metamagnetic system, is M_s. The magnetizations of two sublattices are not equal for $M_s \neq 0$, and the system is in the metamagnetic phase. The magnetizations of two sublattices are equal for $M_s = 0$, and the system is in the saturated paramagnetic phase. Because M_s is small in the neighborhood of second-order transition point, we can expand Eqs. (15) and (16).

The expansion of the longitudinal total magnetization takes the form

$$M_t = M_{t0} + M_{t1} = M_{t0} + B_1M_s^2 + B_2M_s^4 + B_3M_s^6 + B_4M_s^8 + \cdots, \tag{19}$$

where M_{t0} is the paramagnetic solution and is given by equation

$$M_{t0} = \frac{\alpha M_{t0} + h}{\sqrt{(\alpha M_{t0} + h)^2 + \Omega^2}} \tanh \frac{\sqrt{(\alpha M_{t0} + h)^2 + \Omega^2}}{t}, \tag{20}$$

and

$$M_{t1} = B_1M_s^2 + B_2M_s^4 + B_3M_s^6 + B_4M_s^8 + \cdots. \tag{21}$$

Inserting Eq. (19) into Eqs. (15) and (16), and noting αM_{t1} is also small in the neighborhood of second-order transition point, the expansion of the right-hand side of Eqs. (15) and (16) in powers of $(\alpha M_{t1} \pm M_s)$ gives the expressions

$$M_{t1} = \frac{1}{2}\sum_{n=1}^{\infty} A_n[(\alpha M_{t1} + M_s)^n + (\alpha M_{t1} - M_s)^n], \tag{22}$$

$$M_S = \frac{1}{2}\sum_{n=1}^{\infty} A_n[(\alpha M_{t1} + M_s)^n - (\alpha M_{t1} - M_s)^n]. \tag{23}$$

Inserting Eq. (21) into Eq. (22) and equating the coefficients of the same degree in M_s, we find the coefficients B_n in terms of A_n,

$$B_1 = \frac{A_2}{1 - \alpha A_1}, \tag{24}$$

$$B_2 = \frac{1}{1 - \alpha A_1}(\alpha^2 A_2 B_1^2 + 3\alpha A_3 B_1 + A_4), \tag{25}$$

$$B_3 = \frac{1}{1 - \alpha A_1}(2A_2B_1B_2 + 3\alpha A_3B_2 + 6\alpha^2 A_4B_1 + 5\alpha A_5B_1 + 15\alpha^2 A_6B_1^2 + A_6). \tag{26}$$

Finally, substituting M_{t1}, given by Eq. (21), into Eq. (23) we obtain the expansion

$$aM_s + bM_s^3 + cM_s^5 + dM_s^7 + \cdots = 0, \tag{27}$$

where

$$a = 1 - A_1, \tag{28}$$

$$b = -2\alpha A_2 B_1 - A_3, \tag{29}$$

$$c = -2\alpha A_2 B_2 - 3\alpha^2 A_3 B_1^2 - 4\alpha A_4 B_1 - A_5, \tag{30}$$

$$d = -2\alpha A_2 B_3 - 6\alpha^2 A_3 B_1 B_2 - 4\alpha^3 A_4 B_1^3 - 4\alpha A_4 B_2 - 10\alpha^2 A_5 B_1^2 - 6\alpha A_6 B_1 - A_7. \tag{31}$$

The coefficients $A_n(n=1-5)$ are given in the Appendix.

The second-order transition point is found at $a=0$ with $b>0$, the tricritical point occurs for $a=b=0$ with $c>0$, and the fourth-order critical point occurs for $a=b=c=0$ with $d>0$.

III. NUMERICAL RESULTS AND DISCUSSIONS

In this section, we shall present and discuss the results we have obtained for the finite temperature phase diagrams together with the temperature dependence of the staggered magnetization.

In a previous paper,[28] we have given the ground-state phase diagrams of the present model and found that at $\alpha=-0.5$, $h=0.7071$, and $\Omega=0.3536$, $a=b=c=0$. From Eq. (14b), we also know that $\alpha=-0.25$ corresponds to $R=-3/5$, so for $\alpha>-0.25$, there is a tricritical point; for $\alpha<-0.25$, the tricritical point decomposes into a critical end point and a double critical end point when $\Omega=0$.

Some typical results of the finite temperature phase diagram in the Ω-t plane are depicted in Figs. 1 and 2 for $\alpha=0.1$ (>-0.25) and $-0.4(-0.25>\alpha>-0.5)$, respectively. In the phase diagrams, the second-order transition lines, the tricritical points, and the fourth-order critical points are obtained through solving numerically $a=0$ and $b>0$, $a=b=0$ and $c>0$, and $a=b=c=0$ with $d>0$, respectively. Here a, b, c, and d are given by Eqs. (28)–(31). However, the phase transitions of first order must be determined by comparing the corresponding Gibbs free energies of the various solutions of Eqs. (15) and (16) for the pair (M_t, M_s) by using Eq. (18). In the phase diagrams, the solid and dashed lines indicate, respectively, the phase transitions of the second and the first order, the ▲ curve is the tricritical line, and the number accompanying each curve is the value of h.

In Fig. 1, we see that the phase diagram comprises a metamagnetic phase ($m_s \neq 0$) at low transverse fields and a paramagnetic phase ($m_s=0$) at high transverse fields for a fixed value of longitudinal field h. The phase transitions between these phases are of first order for low temperatures, low transverse fields, and high longitudinal fields, and the phase transitions are of second order for high temperatures, high transverse fields, and low longitudinal fields, being separated by the tricritical point. The temperature of the tricritical point monotone increases as the transverse magnetic field Ω decreases and the longitudinal magnetic field h increases. In the region $[0.7607<\Omega<1,\ 0<h<0.2994]$, the phase transition is always of second order. In the region $[0<\Omega<0.5465,\ 0.3689<h<0.45]$, the phase transition is always of first order. In these two regions, the tricritical point does not exist. We also find that the phase transitions change from second order for high temperatures to first order for low temperatures with increasing Ω from 0 to 0.7156 for a given value of $h(0.2994<h<0.3689)$. At $t=0$, $\Omega=0$, comparing the corresponding Gibbs free energies of the various solutions of Eqs. (29) and (30), one can find $h_c=(1-\alpha)/2$. When $h>h_c$, the system is the disorder phase and it is the order phase when $h<h_c$. We can determine $h_c=0.45$ at $t=0$, $\Omega=0$.

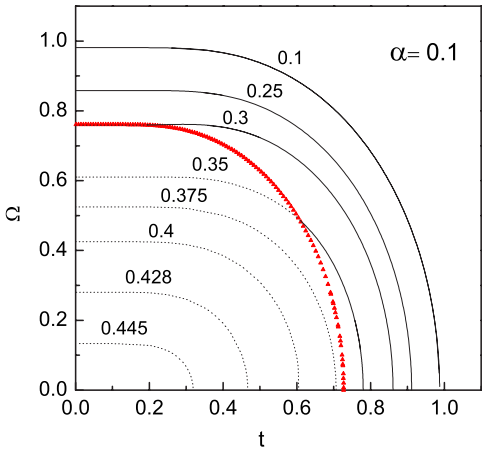

FIG. 1. (Color online) Finite temperature phase diagrams in the Ω-t plane for $\alpha=0.1$. The dashed and the solid curves indicate first-order and second-order transition lines, the ▲ curve is the tricritical line, and the number accompanying each curve is the value of h.

In Fig. 2, we find that for $[0.4517<\Omega<1,\ 0\leqslant h\leqslant 0.6341]$, the phase diagram consists of entirely the lines of

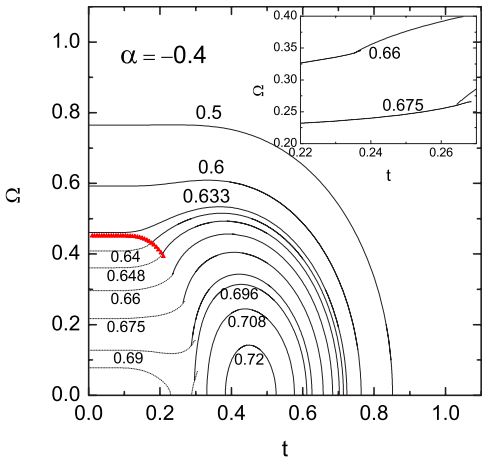

FIG. 2. (Color online) Finite temperature phase diagrams in the Ω-t plane for $\alpha=-0.4$. The dashed and the solid curves indicate first-order and second-order transition lines, the ▲ curve is the tricritical line, and the number accompanying each curve is the value of h.

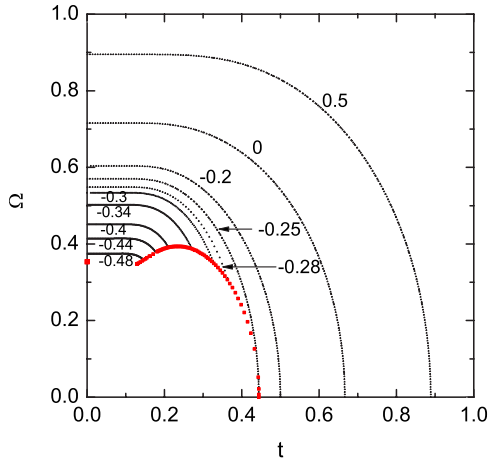

FIG. 3. (Color online) Projection of the tricritical line along the h axis. The ▲ lines represent the positions of stable tricritical points and the ■ line corresponds to the projection of the fourth-order critical points.

second-order points; for $[0.3939<\Omega<0.4517,\ 0.6341<h<0.6492]$, a tricritical point appears and the first-order line joins smoothly to the second-order line. For $[0\leqslant\Omega<0.3939,\ 0.6497<h<0.6976]$, the tricritical point disappears and decomposes into a critical end point and a bicritical end point. A typical phase diagram is shown in the inset of Fig. 2. The fourth-order critical point is located at the intersection of the tricritical line, the line of critical end point, and the line of the bicritical end point. Of most interest is the existence of a fourth-order critical point at $h=0.6497$, $\Omega=0.3908$, $t=0.2108$. When $\Omega=0$, $h_c=0.70$, the system is the disorder phase. For $0.6976<h<0.726$, the transitions again become of second order with the reentrant phenomenon.

In order to see the effect of the field on the tricritical behavior, the projections of the tricritical lines along the h axis are plotted in Fig. 3 for different values of α. In Fig. 3, the ▲ lines represent the positions of stable tricritical points, the ■ line corresponds to the projection of the fourth-order critical points, and the number accompanying each curve is the value of α. In Fig. 3, we see that the tricritical temperature t_r decreases as the Ω increases and the h decreases for a given value of α. The region exhibiting the first-order transition and the length of the tricritical line decrease as the value of α decreases. The fourth-order point appears in the region $-0.5\leqslant\alpha\leqslant-0.25$.

The phase diagrams with fourth-order critical points have been obtained in the mean-field Ising model in the presence of a random field obeying a symmetric three-peak distribution,[29] in the BEG model with a repulsive biquadratic coupling,[30] in the random-site binary ferromagnetic Ising model consisting of spin 1/2 and spin 1 with a single-ion anisotropy,[31] in the mixed spin-1 and spin-3/2 Ising system on a square lattice with different single-ion anisotropies,[32] and in the mean-field Ising model of the mixed ferromagnetic-ferrimagnetic ternary alloy with a single-ion anisotropy.[33] However, in these reference, the single fourth-order critical point in the phase diagrams is given. In the present model, we find the fourth-order critical point line.

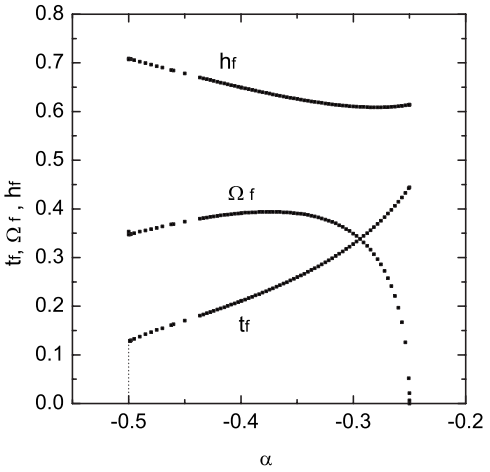

FIG. 4. Positions (t_f,Ω_f,h_f) of the fourth critical order point as a function of α.

Figure 4 shows the position (t_f,Ω_f,h_f) of the fourth-order critical points as a function of α. When $\alpha=-0.25$ $(R=-3/5)$, the position of the fourth critical order point is at $(t_f,\Omega_f,h_f)=(4/9,0,0.614)$; this result is the same as that given in Ref. 15. In the figure, one can find that the Ω_f has the maximum value 0.3937 at $\alpha=-0.3537$ and h_f has the minimum value 0.6088 at $\alpha=-0.2790$. It is necessary to note that the temperature falls to zero, i.e., $t_f=0$, at $\alpha=-0.5$.

Figure 5 expresses the finite temperature phase diagram in the Ω-t plane for $\alpha=-0.6(<-0.5)$. This figure is similar to Fig. 2 except the absence of tricritical point line. We find that for $[0.3507<\Omega<1,\ 0\leqslant h\leqslant0.7781]$, the phase diagram consists of entirely the lines of second-order points; for $[0\leqslant\Omega<0.3507,\ 0.7781<h<0.8000]$, the critical end point and the bicritical end point can be found. A typical phase diagram is shown in the inset. For $0.8002<h<0.8775$, the transitions again become of second order with the reentrant phenomenon.

Figures 6(a)–6(d) express the behaviors of staggered magnetization per site as a function of temperature for the present

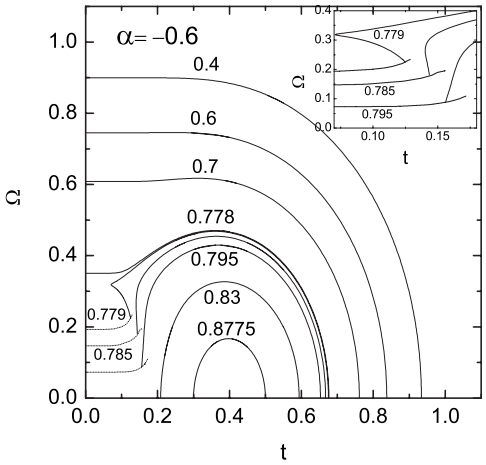

FIG. 5. Finite temperature phase diagram in the Ω-t plane for $\alpha=-0.6$. The dashed and the solid curves indicate first-order and second-order transition lines and the number accompanying each curve is the value of h.

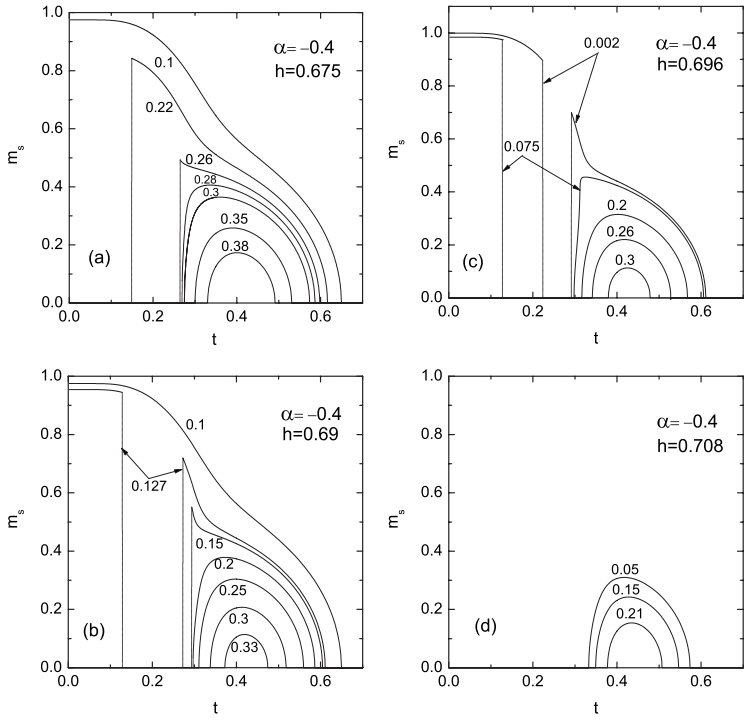

FIG. 6. Thermal variations of the staggered magnetization m_s with $\alpha=-0.4$ for h equal to (a)0.675, (b)0.69, (c)0.696, and (d)0.708. The number accompanying each curve is the value of Ω, and the vertical dashed lines indicate the first-order transitions.

model with $\alpha=-0.4$, $h=0.675, 0.69, 0.696, 0.708$, respectively, when values of Ω are changed. In these figures, the staggered magnetization curves exhibit reentrant phenomena except the curve labeled 0.1. In particular, the staggered magnetization curves labeled 0.127 of Fig. 6(b) and 0.002 of Fig. 6(c) express the characteristic behavior: the staggered magnetization curve is divided into two segments, i.e., with the increase of the temperature t from 0 the staggered magnetization first decreases and suddenly changes to zero, then suddenly increases from 0 to a certain maximum value, and finally continuously decreases to zero again. The staggered magnetization curve labeled 0.075 of Fig. 6(c) expresses similar behavior and is divided into two segments, but in the second segment the staggered magnetization continuously increases from 0 to a certain maximum value. For the given α and h, as Ω increases the first segment of staggered magnetization curve firstly disappears and then the second segment also disappears. The role of transverse field Ω is to destroy the reentrant phenomenon. In other words, when the transverse field is not too large, the reentrant phenomenon becomes weak. When the transverse field is larger than a certain value, the reentrant phenomenon will disappear and the staggered magnetization curve becomes to a point. The positions of the points are at ($\Omega=0.4048$, $t=0.4074$), ($\Omega=0.3428$, $t=0.4212$), ($\Omega=0.3139$, $t=0.4276$), and ($\Omega=0.2446$, $t=0.4383$) for the above four cases. We know that the phase transition line in Fig. 2 changes to be a point located at $\Omega=0$, $t=0$ when $h=0.7$. However in Fig. 6(d), for $h=0.708$, the system exhibits reentrant phenomenon; it is shown that the role of h is to generate the reentrant phenomenon. The curves in Fig. 6 are consistent with the results in Fig. 2.

Finally, in order to compare with previous results, we also give some typical phase diagrams. Figure 7(a) shows the phase diagram of the system for $t=0$, $\alpha=0$ and -1. In Fig.

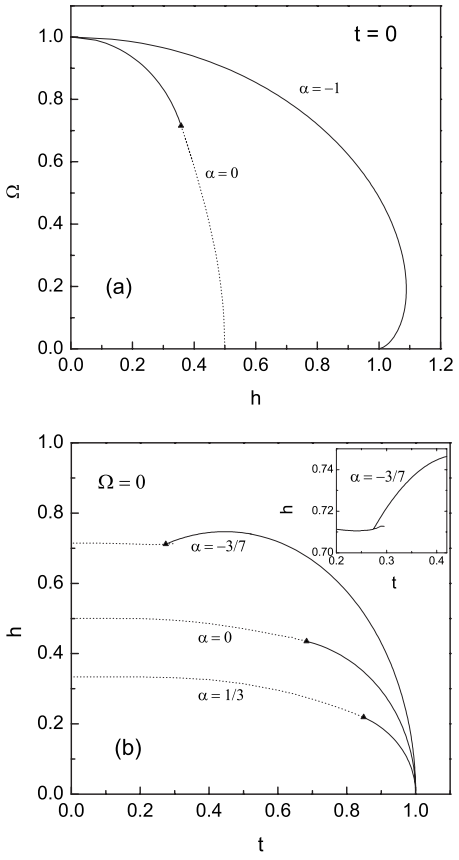

FIG. 7. (a) Ground-state phase diagram in the Ω-h plane for $\alpha=0$ and -1. (b) Finite temperature phase diagrams for $\alpha=0$, $1/3$, and $-3/7$ when $\Omega=0$. The dashed and the solid curves indicate first-order and second-order transition lines, respectively, and ▲ is the tricritical point.

7(a), we can see that the curve labeled $\alpha=-1$ is the same as the one in Ref. 25, which is obtained by using the classical approximation when spins are represented as three-dimension vectors. We can also see that the curve labeled $\alpha=0$ is the same as Fig. 1 of Ref. 34; the position of the tricritical point is at $h_{t0}=4/5^{3/2}=0.3578$, $\Omega_{t0}=8/5^{3/2}=0.7156$. When $h=0$, we see that $\Omega_c=z_1J_1-z_2J_2$ and it is independent of α. Figure 7(b) shows the phase diagrams of the system for $\Omega=0$, $\alpha=0$, $1/3$, and $-3/7$. We can see that the phase transition curve labeled 0 is the same as curve a of Figs. 1 and 2 of Ref. 19; the tricritical point is at $t=0.6667, h=0.4390$. The two phase transition curves labeled $1/3$ ($R=-2$) and $-3/7$ ($R=-0.4$) in Fig. 7(b), after expanding both axis h and axis Ω by 6 and 2.8 times, respectively, are the same as those of Figs. 1 and 3 of Ref. 5.

IV. CONCLUSION

Within the mean-field approach based on Bogoliubov's inequality for the Gibbs free energy, the two-sublattice Ising metamagnet in both external longitudinal and transverse fields is studied. We calculate the staggered magnetization, the longitudinal total magnetization, the transverse total magnetization, the free energy, etc., and plot the finite temperature phase diagrams in the Ω-t plane for some typical parameters. The results show that the tricritical points can occur in a certain region of the external longitudinal and transverse fields and that the temperature of the tricritical point monotone increases with decreasing the transverse magnetic field Ω and increasing the longitudinal magnetic field h. Of most interest is the existence of the fourth-order critical point in the phase diagrams due to the existence of the transverse field Ω. We have found that the fourth-order critical point appears in the region $-0.5 \leqslant \alpha \leqslant -0.25$ and obtained the position of the fourth-order critical point as a function of α. In the phase diagrams, there are various reentrant phenomena. Of course, these results are obtained by using the mean-field theory and need further investigation by using more reliable techniques such as the effective-field theory, Monte Carlo simulation, or renormalization-group approach.

ACKNOWLEDGMENT

This work was supported by the Natural Science Foundation of Liaoning province (Grant No. 20062035).

APPENDIX

The list of coefficients in Eqs. (28)–(31) is as follows.

$$A_1=\frac{\Omega^2}{[(h+\alpha M_{t0})^2+\Omega^2]^{3/2}}\tanh\frac{\sqrt{(h+\alpha M_{t0})^2+\Omega^2}}{t}+\frac{(h+\alpha M_{t0})^2}{t(h+\alpha M_{t0})^2+\Omega^2}\left[1-\tanh^2\frac{\sqrt{(h+\alpha M_{t0})^2+\Omega^2}}{t}\right],$$

$$A_2=-\frac{3\Omega^2(h+\alpha M_{t0})}{2[(h+\alpha M_{t0})^2+\Omega^2]^{5/2}}\tanh\frac{\sqrt{(h+\alpha M_{t0})^2+\Omega^2}}{t}+\frac{3\Omega^2(h+\alpha M_{t0})}{2t[(h+\alpha M_{t0})^2+\Omega^2]^2}\left[1-\tanh^2\frac{\sqrt{(h+\alpha M_{t0})^2+\Omega^2}}{t}\right]$$
$$-\frac{(h+\alpha M_{t0})^3}{t^2[(h+\alpha M_{t0})^2+\Omega^2]^{3/2}}\tanh\frac{\sqrt{(h+\alpha M_{t0})^2+\Omega^2}}{t}\left[1-\tanh^2\frac{\sqrt{(h+\alpha M_{t0})^2+\Omega^2}}{t}\right],$$

$$A_3=\frac{\Omega^2[4(h+\alpha M_{t0})^2-\Omega^2]}{2[(h+\alpha M_{t0})^2+\Omega^2]^{7/2}}\tanh\frac{\sqrt{(h+\alpha M_{t0})^2+\Omega^2}}{t}-\frac{\Omega^2[4(h+\alpha M_{t0})^2-\Omega^2]}{2t[(h+\alpha M_{t0})^2+\Omega^2]^3}\left[1-\tanh^2\frac{\sqrt{(h+\alpha M_{t0})^2+\Omega^2}}{t}\right]$$
$$-\frac{2(h+\alpha M_{t0})^2\Omega^2}{t^2[(h+\alpha M_{t0})^2+\Omega^2]^{5/2}}\tanh\frac{\sqrt{(h+\alpha M_{t0})^2+\Omega^2}}{t}\left[1-\tanh^2\frac{\sqrt{(h+\alpha M_{t0})^2+\Omega^2}}{t}\right]$$
$$-\frac{(h+\alpha M_{t0})^4}{3t^3[(h+\alpha M_{t0})^2+\Omega^2]^2}\left[1-4\tanh^2\frac{\sqrt{(h+\alpha M_{t0})^2+\Omega^2}}{t}+3\tanh^4\frac{\sqrt{(h+\alpha M_{t0})^2+\Omega^2}}{t}\right],$$

$$A_4=\frac{5(h+\alpha M_{t0})\Omega^2[3\Omega^2-4(h+\alpha M_{t0})^2]}{8[(h+\alpha M_{t0})^2+\Omega^2]^{9/2}}\tanh\frac{\sqrt{(h+\alpha M_{t0})^2+\Omega^2}}{t}-\frac{5(h+\alpha M_{t0})\Omega^2[3\Omega^2-4(h+\alpha M_{t0})^2]}{8t[(h+\alpha M_{t0})^2+\Omega^2]^4}$$
$$\times\left[1-\tanh^2\frac{\sqrt{(h+\alpha M_{t0})^2+\Omega^2}}{t}\right]-\frac{5(h+\alpha M_{t0})\Omega^2[\Omega^2-2(h+\alpha M_{t0})^2]}{4t^2[(h+\alpha M_{t0})^2+\Omega^2]^{7/2}}\tanh\frac{\sqrt{(h+\alpha M_{t0})^2+\Omega^2}}{t}$$
$$\times\left[1-\tanh^2\frac{\sqrt{(h+\alpha M_{t0})^2+\Omega^2}}{t}\right]-\frac{5(h+\alpha M_{t0})^3\Omega^2}{6t^3[(h+\alpha M_{t0})^2+\Omega^2]^3}\left[1-4\tanh^2\frac{\sqrt{(h+\alpha M_{t0})^2+\Omega^2}}{t}+3\tanh^4\frac{\sqrt{(h+\alpha M_{t0})^2+\Omega^2}}{t}\right]$$
$$-\frac{(h+\alpha M_{t0})^5}{3t^4[(h+\alpha M_{t0})^2+\Omega^2]^{5/2}}\left[2\tanh\frac{\sqrt{(h+\alpha M_{t0})^2+\Omega^2}}{t}-5\tanh^3\frac{\sqrt{(h+\alpha M_{t0})^2+\Omega^2}}{t}+3\tanh^5\frac{\sqrt{(h+\alpha M_{t0})^2+\Omega^2}}{t}\right],$$

$$A_5 = \frac{3\Omega^2[\Omega^4 - 12\Omega^2(h+\alpha M_{t0})^2 + 8(h+\alpha M_{t0})^4]}{8[(h+\alpha M_{t0})^2+\Omega^2]^{11/2}} \tanh\frac{\sqrt{(h+\alpha M_{t0})^2+\Omega^2}}{t} - \frac{3\Omega^2[\Omega^4 - 12\Omega^2(h+\alpha M_{t0})^2 + 8(h+\alpha M_{t0})^4]}{8t[(h+\alpha M_{t0})^2+\Omega^2]^5}$$
$$\times\left[1-\tanh^2\frac{\sqrt{(h+\alpha M_{t0})^2+\Omega^2}}{t}\right] - \frac{\Omega^2[\Omega^4 - 15\Omega^2(h+\alpha M_{t0})^2 + 12(h+\alpha M_{t0})^4]}{4t^2[(h+\alpha M_{t0})^2+\Omega^2]^{9/2}} \tanh\frac{\sqrt{(h+\alpha M_{t0})^2+\Omega^2}}{t}$$
$$\times\left[1-\tanh^2\frac{\sqrt{(h+\alpha M_{t0})^2+\Omega^2}}{t}\right] + \frac{\Omega^2(h+\alpha M_{t0})^2[4(h+\alpha M_{t0})^2 - 3\Omega^2]}{4t^3[(h+\alpha M_{t0})^2+\Omega^2]^4}\left[1-4\tanh^2\frac{\sqrt{(h+\alpha M_{t0})^2+\Omega^2}}{t}\right.$$
$$\left.+3\tanh^4\frac{\sqrt{(h+\alpha M_{t0})^2+\Omega^2}}{t}\right] + \frac{\Omega^2(h+\alpha M_{t0})^4}{t^4[(h+\alpha M_{t0})^2+\Omega^2]^{7/2}}\left[2\tanh\frac{\sqrt{(h+\alpha M_{t0})^2+\Omega^2}}{t} - 5\tanh^3\frac{\sqrt{(h+\alpha M_{t0})^2+\Omega^2}}{t}\right.$$
$$\left.+3\tanh^4\frac{\sqrt{(h+\alpha M_{t0})^2+\Omega^2}}{t}\right] + \frac{(h+\alpha M_{t0})^6}{15t^5[(h+\alpha M_{t0})^2+\Omega^2]^3}\left[2-17\tanh^2\frac{\sqrt{(h+\alpha M_{t0})^2+\Omega^2}}{t} + 30\tanh^4\frac{\sqrt{(h+\alpha M_{t0})^2+\Omega^2}}{t}\right.$$
$$\left.-15\tanh^6\frac{\sqrt{(h+\alpha M_{t0})^2+\Omega^2}}{t}\right],$$

A_6 and A_7 are not given here for simplicity.

*Corresponding author; guozhuwei02@sina.com

[1] J. M. Kincaid and E. G. D. Cohen, Phys. Rep., Phys. Lett. **22C**, 57 (1975).
[2] H. J. Herrmann, E. B. Rasmusseen, and D. P. Landau, J. Appl. Phys. **53**, 7994 (1982).
[3] D. P. Landau and R. H. Swendsen, Phys. Rev. Lett. **46**, 1437 (1987).
[4] H. J. Herrmann and D. P. Landau, Phys. Rev. B **48**, 239 (1993).
[5] W. Selke, Z. Phys. B: Condens. Matter **101**, 145 (1996).
[6] M. Pleimling and W. Selke, Phys. Rev. B **56**, 8855 (1997).
[7] M. Santos and W. Figueiredo, Phys. Rev. B **58**, 9321 (1998).
[8] M. Žukovič and A. Bobak, J. Magn. Magn. Mater. **170**, 49 (1997).
[9] M. Žukovič and T. Idogaki, J. Magn. Magn. Mater. **208**, 120 (2000).
[10] A. F. S. Moreira, W. Figueiredo, and V. B. Henriques, Phys. Rev. B **66**, 224425 (2002).
[11] V. A. Schmidt and S. A. Friedberg, Phys. Rev. B **1**, 2250 (1970).
[12] E. Stryjewski and N. Giordano, Adv. Phys. **26**, 487 (1977).
[13] K. Katsumata, H. A. Katori, S. M. Shapiro, and G. Shirane, Phys. Rev. B **55**, 11466 (1997).
[14] W. P. Wolf, Braz. J. Phys. **30**, 794 (2000).
[15] J. M. Kincaid and E. G. D. Cohen, Phys. Lett. **50**, 317 (1974).
[16] Y. L. Wang and K. Rauchwarger, Phys. Lett. **59**, 73 (1974).
[17] Y. L. Wang and J. D. Kimel, J. Appl. Phys. **69**, 6176 (1991).
[18] M. Žukovič and T. Idogaki, Phys. Rev. B **61**, 50 (2000).
[19] S. Galam, C. S. O. Yokoi, and S. R. Salinas, Phys. Rev. B **57**, 8370 (1998).
[20] O. Petracic, Ch. Binek, W. Kleemann, U. Neuhausen, and H. Lueken, Phys. Rev. B **57**, R11051 (1998).
[21] B. H. Teng and H. K. Sy, Physica B **348**, 485 (2004).
[22] T. Kaneyoshi, E. F. Sarmento, and I. P. Fittipaldi, Phys. Rev. B **38**, 2649 (1988).
[23] T. Kaneyoshi, Physica A **319**, 355 (2003).
[24] W. Jiang, G. Z. Wei, and Z. H. Xin, Physica A **293**, 455 (2001).
[25] A. A. Ovchinnikov, D. V. Dmitriev, V. Y. Krivnov, and V. O. Cheranovskii, Phys. Rev. B **68**, 214406 (2003).
[26] H. Falk, Am. J. Phys. **38**, 858 (1970).
[27] T. Kaneyoshi, M. Jascur, and I. P. Fittipaldi, Phys. Rev. B **48**, 250 (1993).
[28] J. Liu, G. Z. Wei, H. L. Miu, and A. Du, J. Magn. Magn. Mater. (to be published).
[29] M. Kaufman, P. E. Klunzinger, and A. Khurana, Phys. Rev. B **34**, 4766 (1986).
[30] W. Hoston and A. N. Berker, Phys. Rev. Lett. **67**, 1027 (1991).
[31] J. A. Plascak, Physica A **198**, 655 (1993).
[32] A. Bobak, Physica A **286**, 531 (2000).
[33] A. Bobák, F. O. Abubrig, and T. Balcerzak, Phys. Rev. B **68**, 224405 (2003).
[34] F. S. Milman, P. R. Hauser, and W. Figueiredo, Phys. Rev. B **43**, 13641 (1991).